Int J Adv Manuf Technol (1999) 15:683–691

The International Journal of
Advanced
Manufacturing
Technology

Model-Based Motion Planning for Robotic Assembly of Non-Cylindrical Parts

Y. L. Yao[1] and W. Y. Cheng[2]

[1]Department of Mechanical Engineering, Columbia University, New York, USA; and [2]Department of Mechanical Engineering, University of Wollongong, Wollongong, Australia

In high-speed part mating using robotic arms, the dynamic characteristics of the mating process have to be considered. This paper first derives the geometrical compatibility condition for the insertion motion where mating force/moment are free of overshooting. Simulation studies are then carried out where the dynamic characteristics of a robot, subjected to contact force and moment, are formulated and solved numerically. On that basis, the worst case among different types and combinations of misalignments is predicted and a varying speed insertion motion is synthesised. Experimental investigations involving square peg mating using a SCARA robot are presented. The experimental results show that with such a varying-speed motion, assembly operations can be carried out in a reduced cycle time without inducing excessive contact force and moments.

Keywords: Misalignment, Part mating; Robotic assembly; SCARA robot

1. Introduction

In recent decades, growth in productivity and improvement in quality consistency have been provided through the use of new technological methods and machines. One area is the increasing application of industrial robots in many assembly processes where peg–hole mating is the most basic and important form of operations. However, variations due to part tolerances as well as robot inaccuracy have led to uncertainties in end-effector position relative to a fixture.

Although, these uncertainties can be accounted for by using active methods such as tactile and vision sensors or passive methods such as a remote centre compliance (RCC), the complexity introduced and the additional cost involved have limited their widespread usage. In addition, such sensors or devices are usually suitable only for a limited class of parts and operating conditions. Therefore, for a given task, it seems logical to consider first whether an available robot can accomplish the task without using special sensors or additional compliance devices [1,2]. ElMaraghy et al. [3] presented a method to examine the adequacy of part dimensional tolerances and robot repeatability for automatic assembly of an existing design. Given the nominal dimension and tolerance of the peg and hole, as well as the repeatability of the robot, the effective clearance and a positioning design factor for assembly can be found.

If the positioning design factor indicates that the combination of tolerance and repeatability is adequate for a given task, no additional sensors or compliant devices are required. The next question is how fast the task can be accomplished, because robot assembly normally entails repetitive tasks and a small saving in each cycle time can be significant. Misalignment and misorientation between parts during automatic assembly, however, can generate excessive contact forces/moments if the insertion speed is too high (Fig. 1). This may lead to damage to the parts and can sometimes stall the assembly manipulator. To avoid this problem, a relatively lower speed is commonly used in mating. This justifies the assumption that the motion takes place in a quasi-static manner. This assumption has been made by many researchers and a good example is work on peg/hole variety by Nevins and Whitney [4]. However, in order to achieve high-speed operations, dynamic characteristics during part mating need to be taken into consideration.

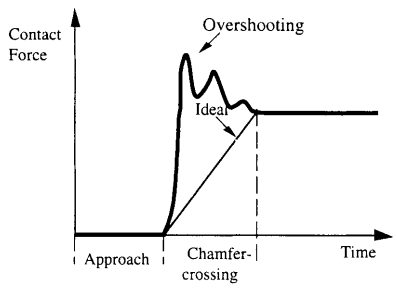

Fig. 1. Excessive and ideal contact force/moment.

Correspondence and offprint requests to: Dr L. Yao, Department of Mechanical Engineering, Columbia University, 220 S.W. Mudd, Mail Code 4703, 500 West 120th Street, New York, NY 10027, USA. E-mail: ylyl@columbia.edu

Research has been reported in the dynamic aspects of part mating [1,5–7].

The strategy presented by Asada and Kakumoto [5] uses a dynamic RCC hand for cylindrical part mating. It focuses on the inertial forces rather than on the static spring forces. The requirement for the desired peg trajectory is to maintain an upright orientation while the peg slides along the chamfer. It is shown that an arbitrary force acting on the general centroid yields only a transitional acceleration. Furthermore, a no-bouncing condition is derived, which states that the angle of the velocity vector from the axis of a hole should not be larger than the angle of the chamfer surface. Yao [1] proposed a varying-speed insertion method for cylindrical part mating. First, the lateral response of the end-effector is predicted by dynamic simulation and a varying-speed insertion motion is synthesised to ensure a mating force free of overshooting. Experimental results demonstrated that the method achieved a reduced insertion cycle time without causing excessive contact forces. Meitinger and Pfeiffer [7] report a dynamic simulation which shows that for compliantly supported part mating, the forces are dependent only on the position and the velocity of the robot's end-effector with respect to the environment, and for relatively rigid part mating, the dynamics of the robots are characterised by closed loops.

Most work on robotic assembly deals with cylindrical part/hole mating, while some attention has been paid to non-cylindrical part mating as it finds applications in microelectronics and other industries [8–14]. Strip [10,11] developed an approach to the insertion of arbitrary convex-shaped pegs into correspondingly shaped holes. First, hybrid force-position control is presented. The insertion procedure begins in a similar manner to that of Caine et al. [9]. The peg is tilted to increase the number of configurations in which the peg will at least enter the hole. The remainder of the strategy is based on the methods used by human operators. Wu and Hopkins [12] present the use of hybrid control for the assembly of a spline peg and a hole. Three-dimensional displacements, rotations, forces and torques are the parameters for the path of insertion, which is divided into approach stage, searching stage I, chamfer crossing stage and searching stage II. This method needs a longer time for searching. Sturges and Laowattana [13] report development of a passive compliance device known as spatial remote centre compliance (SRCC) for use with non-axisymmetric rigid parts, such as, prismatic insertions, and threaded fits. The same authors [15] report design of an orthogonal compliance for polygonal peg insertion.

Similar to Yao [1] and Leu and Jia [2], this paper is concerned with robot mating of rigid non-cylindrical parts using its own compliance. The objectives are to plan the insertion motion such that no excessive contact force/moment occurs while the task is accomplished in the shortest possible cycle time. Non-cylindrical part/hole combinations could be axisymmetric and non-axisymmetric. Square chamfered pegs and holes are dealt with in this paper for simplicity so that the work could be concentrated on deriving conditions for mating force free of overshooting and for higher cycle times.

2. Geometrical Compatibility and Dynamic Characteristics

First, possible cases of misalignments are analysed in order to determine the worst case scenario later in the paper. The geometric compatibility conditions between allowable insertion displacement and the lateral and rotary deflections of the robot's end-effector are then derived. The transient lateral and rotational deflections are determined via simulation of the robot dynamics. A varying-speed motion is finally synthesised and implemented for reduced cycle time and overshoot-free mating.

2.1 Misalignments

It is appropriate to regard cylindrical peg and hole mating as a 2D problem. In the case of a square peg and hole mating, where rotational misalignments could affect the state of contact significantly, the problem must be analysed in 3D. In the following, it is assumed that the hole is rigid and fixed to the ground and the peg is compliantly supported. The centre of the rotational compliance is situated on the axis of insertion (i.e. z-axis in Fig. 2). The rotational misalignments around the x- and y-axes are neglected because most assembly robots (i.e. selective compliance assembly robot arm (SCARA) type) essentially provide one degree of compliance in the horizontal plane. Three cases may be identified, that is, translational misalignment, rotational misalignment, and combined translational and rotational misalignment.

1. *Translational misalignment only*. If only translational misalignment is involved, a line contact occurs between the chamfer and the edge of the hole, as shown in Figs 2(*a*) to 2(*c*). The contact force is evenly distributed along the contact line, and no moment is induced. This can be further divided into three cases:

   Translational misalignment in one direction only (Fig. 2*a*).

   Translational misalignment in both directions by an equal amount (Fig. 2*b*).

   Translational misalignment in both directions by a different amount (Fig. 2*c*).

2. *Rotational misalignment only*. If only rotational misalignment is involved, a 4-point contact occurs, as shown in Fig. 2(*d*). A moment is induced while the resultant of all forces is equal to zero.
3. *Translational and rotational misalignments*. The translational misalignment in two directions could be equal (Fig. 2*e*) or not equal (Fig. 2*f*).

Although the case shown in Fig. 2(*f*) has both rotational and different amounts of translational misalignments present, it may not be the worst case in terms of meeting the requirement of contact force/moment free of overshooting and with reduced assembly cycle time. It will be shown in a later section that the interaction between the robot response and the amount/type of misalignment involved determines which one is the worst case.

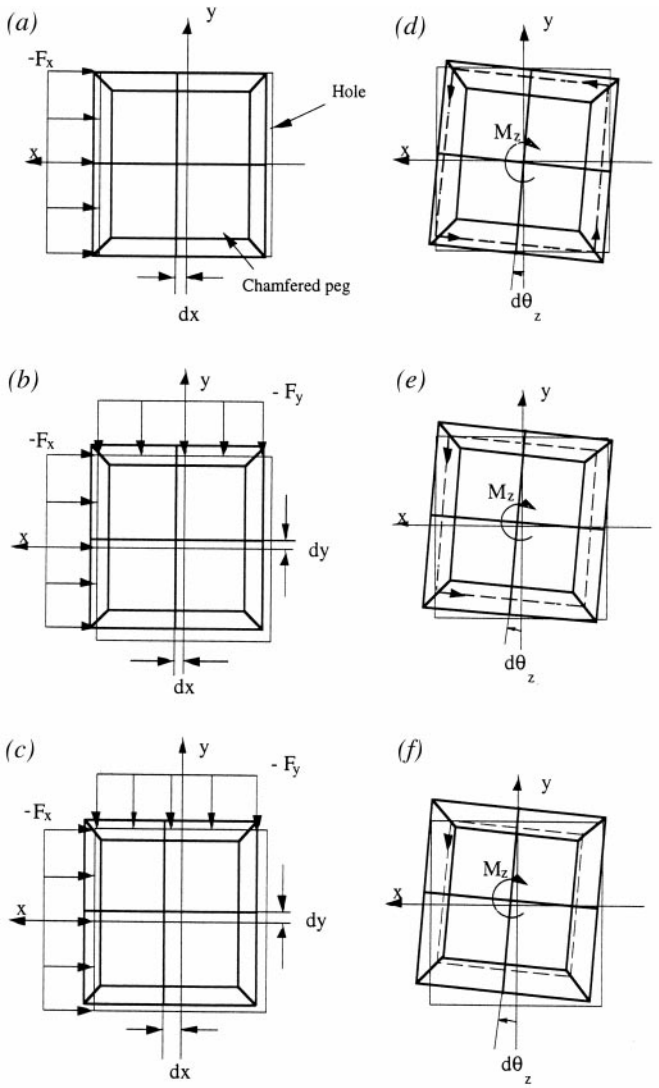

Fig. 2. Possible misalignment combinations for square peg/hole. (*a*) Translational misalignment only (dx or dy). (*b*) Translational misalignment only (dx = dy). (*c*) Translational misalignment only [(dx > dy) or (dy > dx)]. (*d*) Rotational misalignment only. (*e*) Translational and rotational misalignment (dx = dy). (*f*) Translational and rotational misalignment [(dx > dy) or (dy < dx)].

2.2 Geometrical Compatibility for Chamfer-Crossing Motion without Force Overshooting

In deciding the highest speed at which a square peg can be inserted without incurring overshooting in contact force and moment, the insertion motion $\Delta z(t)$ has to be determined according to the end-effector's lateral and orientational dynamic response to the contact force and moment. It is the response which allows the peg into the hole (Fig. 3). The faster the lateral and the orientational response, the faster a part can be inserted. If the peg is inserted too fast, the mating elements will be over stressed and a contact force/moment will momentarily arise and may cause damage to the mating elements.

The allowable insertion, $\Delta z_t(t)$, corresponding to the end-effector's translational response, $\Delta x(t)$ and $\Delta y(t)$, can be shown to be:

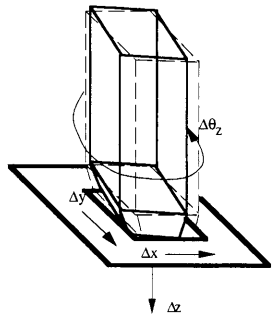

Fig. 3. Lateral response Δx and Δy, rotational response $\Delta\theta_z$ and insertion motion Δz.

$$\Delta z_t(t) = \min\{\Delta x(t), \Delta y(t)\}\tan\alpha \tag{1}$$

where α is the chamfer angle. $\Delta z_t(t)$ is determined according to the smaller of the end-effector's response $\Delta x(t)$ and $\Delta y(t)$ and in this way although conservative, no force overshooting will occur.

Secondly, the allowable insertion $\Delta z_r(t)$, corresponding to the rotational response of a robot, is considered. The side and top views of the peg and hole relation are shown in Figs 4(*a*) and 4(*b*), respectively. The lift-up of the peg in the z-direction, $z_r(t)$, due to the rotational misalignment between the peg and the hole, $\theta_z(t)$, can be shown to be:

$$z_r(t) = \frac{b\,\tan\alpha}{2}\left(1 - \frac{1}{\cos\theta_z(t) + \sin\theta_z(t)}\right) \tag{2}$$

where b is the width of the square peg.

Differentiating both sides of Eq. (2) with respect to time t, one obtains

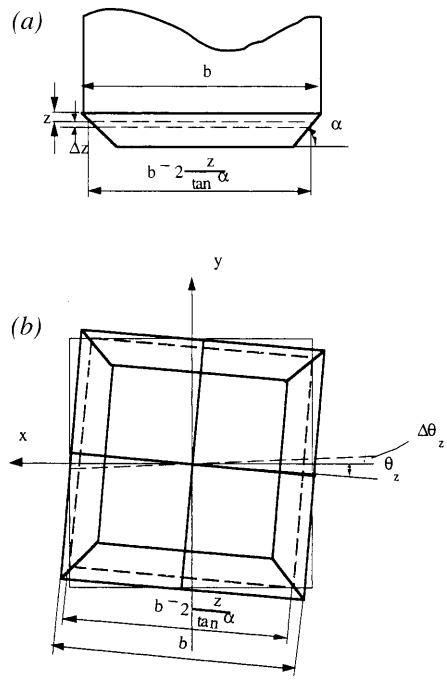

Fig. 4. Illustration for derivation of Eqs (1) to (4). (*a*) Side view. (*b*) Top view.

$$\Delta z_r(t) = \frac{b\,\tan\alpha(\cos\theta_z - \sin\theta_z)}{2(\cos\theta_z+\sin\theta_z)^2}\Delta\theta_z(t) \quad (3)$$

Note that θ_z is the instantaneous rotational misalignment about the z-axis in $\{H\}$ while $d\theta_z$ in Fig. 2 is the maximum rotational misalignment and $\Delta\theta_z$ is the incremental angular displacement at time t. Equation (3) defines the relationship between the rotational response $\Delta\theta_z$ and the corresponding allowable insertion $\Delta z_r(t)$. The total insertion, $\Delta z(t)$, is equal to the sum of Eqs (2) and (3), i.e.

$$\Delta z(t) = \min\{\Delta x(t),\Delta y(t)\}\tan\alpha + \frac{b\,\tan\alpha(\cos\theta_z - \sin\theta_z)}{2(\cos\theta_z + \sin\theta_z)^2}\Delta\theta_z(t) \quad (4)$$

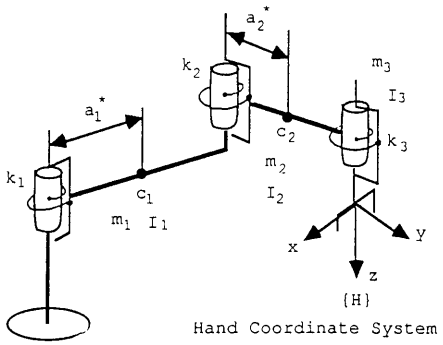

Fig. 5. Simplified model of a SCARA robot.

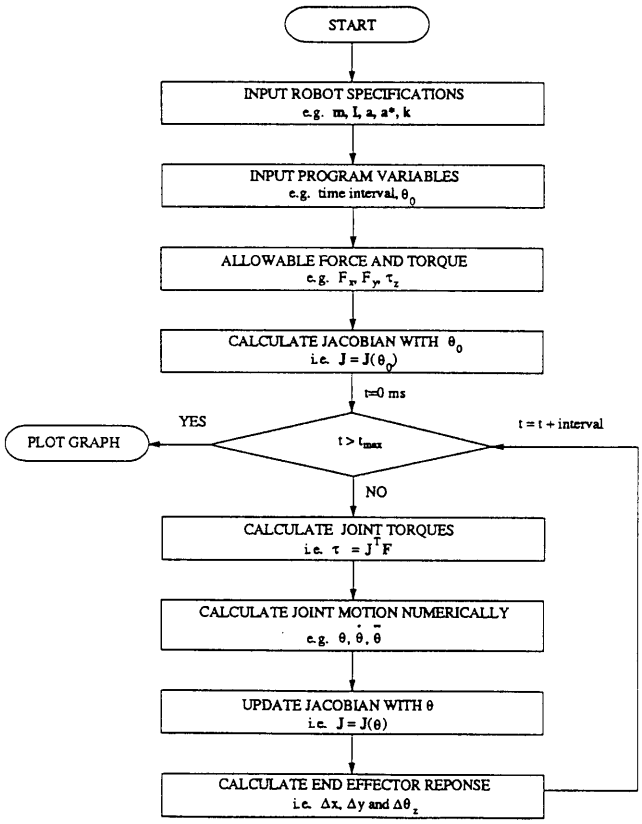

Fig. 6. Flow chart of simulation.

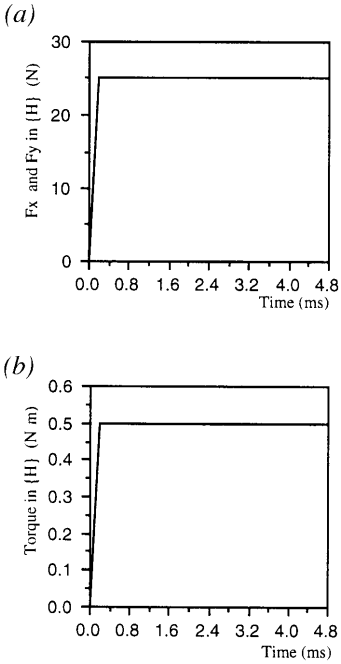

Fig. 7. Contact force/torque in $\{H\}$.

Equation (4) is the basis for synthesising a varying speed insertion motion $\Delta z(t)$ for a square peg and hole mating problem where both translational response $\Delta x(t)$, $\Delta y(t)$ and rotational response $\Delta\theta_z$ are present. An insertion motion synthesised in this way would not result in contact force/moment with overshooting, while achieving a higher possible cycle time under the constraints. The $\Delta x(t)$, $\Delta y(t)$ and $\Delta\theta_z(t)$ required in Eq. (4) are obtained through the dynamic modelling outlined below.

2.3 Dynamic Characteristics of Chamfer-Crossing Motion

To predict $\Delta x(t)$, $\Delta y(t)$ and $\Delta\theta_z(t)$ during the chamfer-crossing stage, a dynamic model is derived. For most assembly tasks, SCARA robots are used. Figure 5 illustrates a simplified model of a SCARA robot. Three rotational joints are modelled which are parallel to each other. With the SCARA design, the robot arms are normally large and can be regarded as rigid links and compliance is primarily due to the joint flexibility. Since the SCARA robot provides a single degree of compliance in the horizontal plane, joint stiffness is simply modelled as a spring, and controller stiffness is not considered here. The bearings are also assumed to be rigid because the joints have larger deflections in comparison [16].

For a mating process by a SCARA robot, a peg is usually carried to a location above the hole by the three rotational joints of the robot, then insertion in the z-direction is activated. Therefore, joints 1 to 3 are held stationary by their motors during insertion and joint rotational deflections are due to joint compliance only. Suppose the joint angles before contacting the chamfer are $\theta_0 = [\theta_{10},\theta_{20},\theta_{30}]^T$ and the joint stiffness

$\mathbf{k} = [k_1,k_2,k_3]^T$, the vector/matrix dynamics written in the joint space is

$$\mathbf{M}(\theta)\ddot{\theta} + \mathbf{V}(\theta,\dot{\theta}) + \mathbf{K}(\theta,\theta_0) = \tau(t) \tag{5}$$

where $\theta = [\theta_1,\theta_2,\theta_3]^T$ are instantaneous joint variables, $\mathbf{M}(\theta)$ is a 3×3 symmetric inertia matrix and $\mathbf{V}$ is 3×1 vector of centrifugal and Coriolis terms. The difference between the above formulation and previous dynamics formulations is in the third term where

$$\mathbf{K}(\theta,\theta_0) = [k_1(\theta_1 - \theta_{10}),k_2(\theta_2 - \theta_{20}),$$
$$k_3(\theta_3 - \theta_{30})]^T \tag{6}$$

The gravitational term is not included because the links remain at the same level all the time.

For a given robot, modelling can be carried out as follows. First, allowable contact forces $F_x(t)$, $F_y(t)$ and torque $\tau_z(t)$ are specified in the hand coordinate system $\{H\}$ and corresponding joint torques $\tau(t) = [\tau_1,\tau_2,\tau_3]^T$ are calculated as

$$\tau(t) = \tau_\alpha(t) + \mathbf{J}_H^T(t)[F_x(t),F_y(t),\tau_z(t)]^T \tag{7}$$

where $\tau_\alpha(t)$ represents a vector of torques generated by joint actuators and $\mathbf{J}_H(t)$ is the 3×3 Jacobian matrix written in $\{H\}$. A numerical method can be applied to solve the differential equation in Eq. (5) for given values of $\tau(t)$ (Eq. (7)) and the results are then converted to $\{H\}$ by

$$[\Delta x(t),\Delta y(t),\Delta\theta_z(t)] = \mathbf{J}_H(t)\Delta\theta(t) \tag{8}$$

and

$$[\Delta\dot{x}(t),\Delta\dot{y}(t),\Delta\dot{\theta}_z(t)] = \mathbf{J}_H(t)\Delta\dot{\theta}(t) \tag{9}$$

where t indicates the time-varying nature of the Jacobian matrix; but it will be seen in the next section that the matrix remains almost constant for small changes of joint angles. The end-effector lateral deflection and rotation $[\Delta x(t),\Delta y(t),\Delta\theta_z(t)]$ expressed in $\{H\}$ can then be used in Eq. (4) to calculate allowable insertion motion, $\Delta z(t)$. The flowchart shown in Fig. 6 summarises the simulation procedure. Since most SCARA robots provide only limited joint compliance, the joint angular deflections when subjected to the end-effector force/moment are usually very small, so that the system non-linearity can be neglected, and therefore using Eqs (8) and (9) is appropriate.

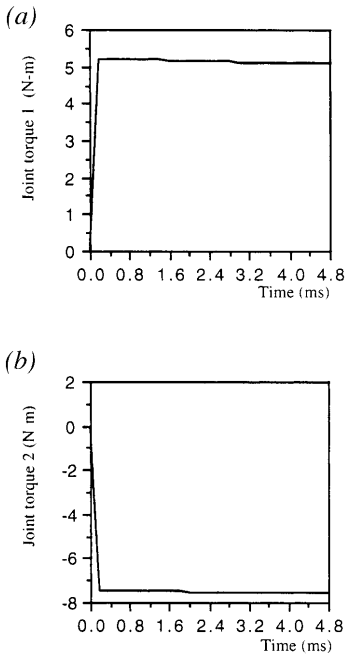

Fig. 8. Corresponding torques in each joint.

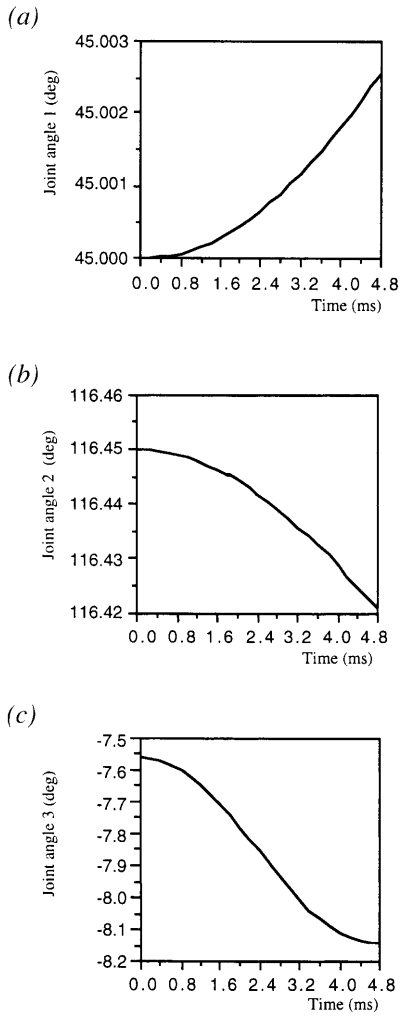

Fig. 9. Joint angular deflections.

3. Simulation

The purpose of the simulation is twofold. First, it is to predict the response Δx, Δy and $\Delta\theta_z$ of a robot's end-effector when it is subject to a given set of contact forces/moments. The prediction is carried out by solving the chamfer-crossing dynamics (Eq. (5)) numerically. Secondly, it is to investigate the worst case among the various misalignments or their combinations identified in Fig. 2, as the basis for synthesising a varying-speed insertion motion. An IBM 7545 robot was

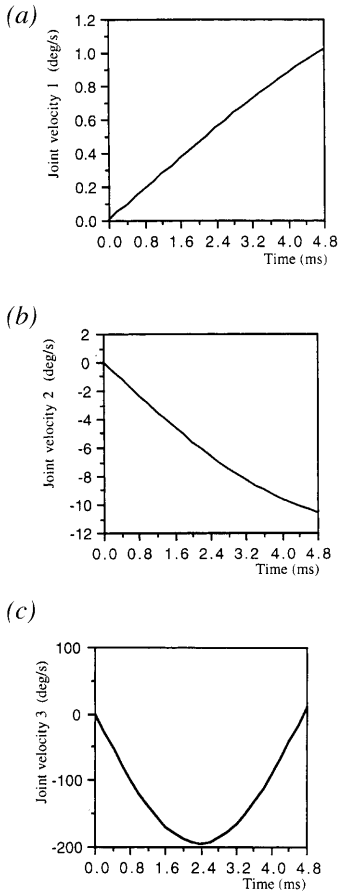

Fig. 10. Joint angular deflection rates.

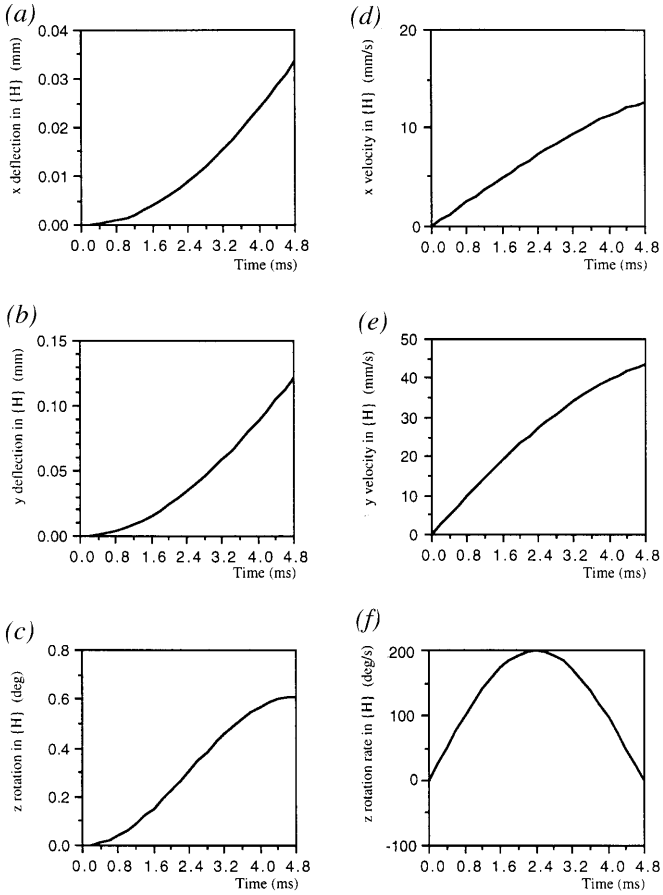

Fig. 11. End effector responses Δx, Δy and $\Delta\theta_z$.

used for the simulation. It is of the SCARA type whose inertia matrix **M** and centrifugal and Coriolis terms **V** are listed in Appendix A.1. Its geometric and inertia parameters are listed in Appendix A.2 and its Jacobian matrix in Appendix A.3.

3.1 The End-Effector's Dynamic Response

First, allowable step contact force and moment inputs $F_x(t)$, $F_y(t)$ and $\tau_z(t)$ of various step sizes were investigated. Presented in Figs 7 to 11 is a case where $F_x = F_y = 25$ N and $\tau_z = 0.5$ N-m were assumed. The inputs were transformed to the joint space using Eq. (7) and the corresponding torques τ_1, τ_2 and τ_3 were obtained as shown in Fig. 8. As seen, the joint torques remain almost constant because the robot configuration change due to the force/moment acting at its end-effector is so small, and consequently its Jacobian remains nearly unchanged during the operation. Joint deflections from the initial configuration, $\theta_{10} = 45°$, $\theta_{20} = 116.45°$ and $\theta_{30} = -7.56°$ shown in Fig. 9 and their derivatives in Fig. 10 were obtained by solving the coupled nonlinear differential equations in Eq. (5) using the 5th-order Runge–Kutta–Verner method. As seen, joints do not deflect instantaneously owing to link inertia among other dynamic effects. The rate of deflection (i.e. joint velocity shown in Fig. 10) is slowest for joint 1 and second slowest for joint 2 because of the progressively increasing inertia effect towards the base of the robot. Finally, the end-effector responses $\Delta x(t)$, $\Delta y(t)$ and $\Delta\theta_z(t)$, as well as their derivatives, are arrived at using Eqs (8) and (9) (Fig. 11). As seen, both the lateral responses $\Delta x(t)$ and $\Delta y(t)$ and rotational response $\Delta\theta_z(t)$ to the step input of contact forces and moment are not instantaneous and the rate of response in x is only about one tenth of that in the y-direction for this robot configuration. The simulation program can predict such responses for any feasible configurations.

3.2 Synthesis of a Varying-Speed Insertion Motion

The end-effector response Δx, Δy and $\Delta\theta_z$ obtained from the simulation is then used to synthesise a varying-speed insertion motion Δz according to Eq. (4). Shown in Fig. 12 are the synthesised Δz results for various possible combinations of translational and rotational misalignments depicted in Fig. 2. For instance, case (*h*) is the synthesised varying speed insertion motion profile when both translational misalignments are assumed to be present and are the same and rotational misalignment is also present. The results show that the simulation produces higher insertion rates for some types and combinations of misalignments, and lower rates for others. In reality, the type and combination of misalignment present in a mating operation is unpredictable. However, if the lowest rate syn-

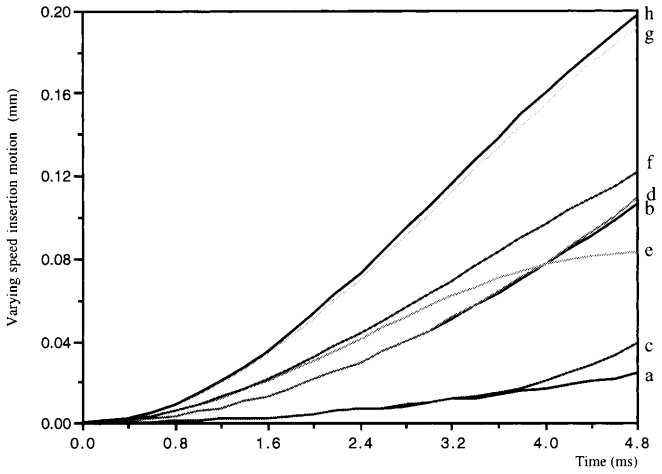

Fig. 12. Varying speed insertion motion synthesized for different types and combinations of misalignments. (*a*) dx only, (*b*) dy only, (*c*) dx > dy, (*d*) dy > dx, (*e*) dθ_z only, (*f*) dx > dy and dθ_z, (*g*) dy > dx and dθ_z, and (*h*) dx = dy and dθ_z.

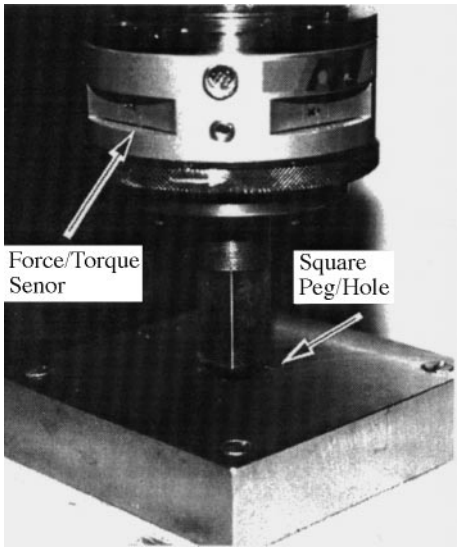

Fig. 13. Square peg-hole mating experiment.

thesised is chosen in insertion planning, contact force and moment free of overshooting can be expected, regardless of which type and combination of alignment is actually present in the mating operation. In this case, as seen from Fig. 12, situation *a* allows the slowest insertion motion and therefore represents the worst case. As a result, the curve corresponding to situation *a* is chosen as the answer. In this way, although conservative, overshooting in contact force and moment is prevented and subsequently the mating elements are protected from impact damage. Note the results here are affected by many factors including robot configuration but the simulation can be conveniently run for a variety of conditions.

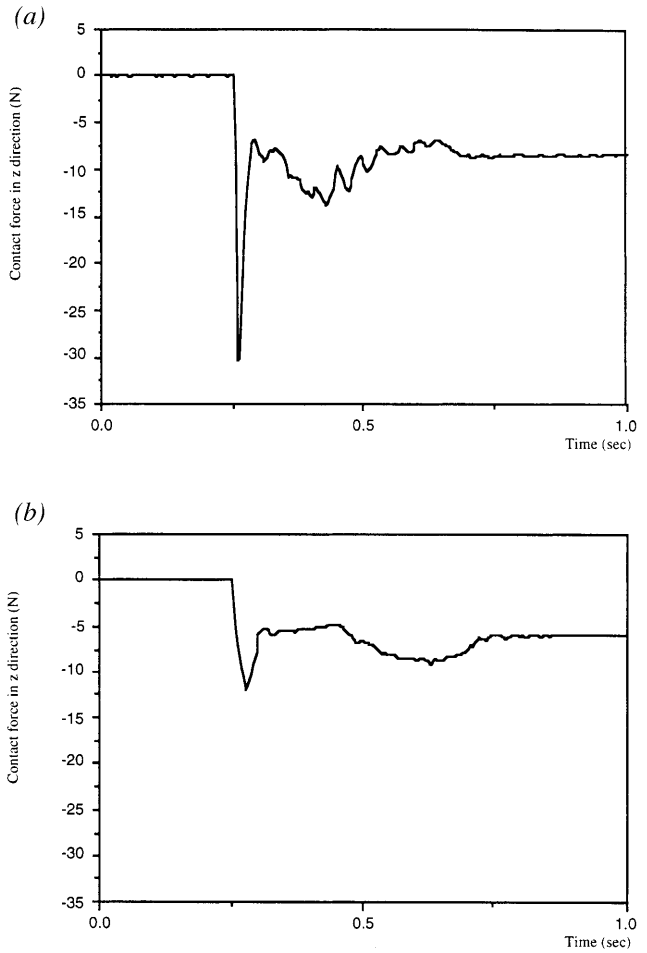

Fig. 14. Experimental comparison of contact force (*a*) using constant speed insertion motion; (*b*) using varying speed insertion motion.

4. Experimental Results and Discussion

The goal of the experiments is to implement the varying-speed insertion method and to compare it with the conventional constant-speed insertion method in terms of contact forces and moments, as well as cycle times.

Experiments involving mating of a chamfered square peg into a square hole made by EDM were conducted. To measure the contact forces and moments during the chamfer-crossing stage, a force and torque sensor (Lord Model 15/100) was mounted behind the peg (Fig. 13). This particular unit is capable of measuring the contact force in three orthogonal directions up to 15 lb. (66.89 N) each and three torque components up to 50 in lb (5.649 N m) each, with little cross-talk. Insertions were programmed for both the varying speed motion and constant speed motion.

In the constant-speed insertion, a speed equal to 5% of the full speed of the robot was programmed for both the approaching and chamfer-crossing stage. The graph (Fig. 14*a*) shows that an excessive contact force was induced at the initial contact. In the varying-speed insertion, the peg was inserted in 100% of the full speed in the approach stage and was made to stop just before it touched the chamfer. Then insertion was

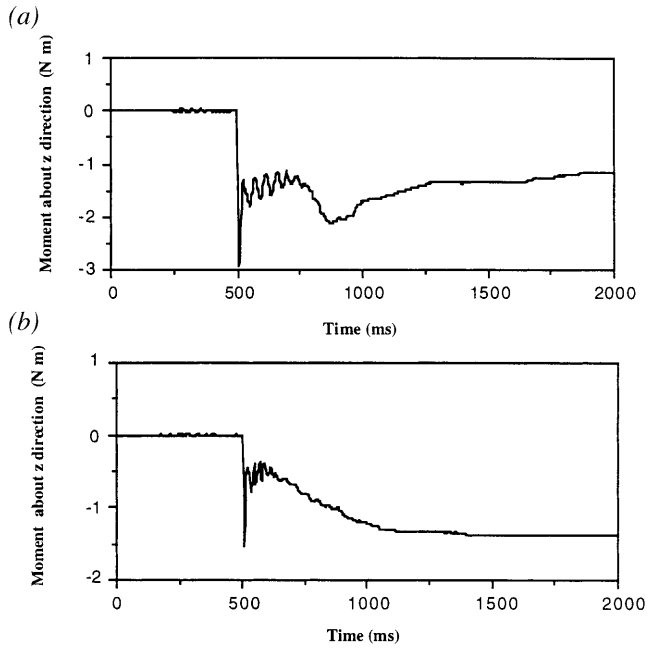

Fig. 15. Experimental comparison of contact moment (*a*) using constant speed insertion motion; (*b*) using varying speed insertion motion.

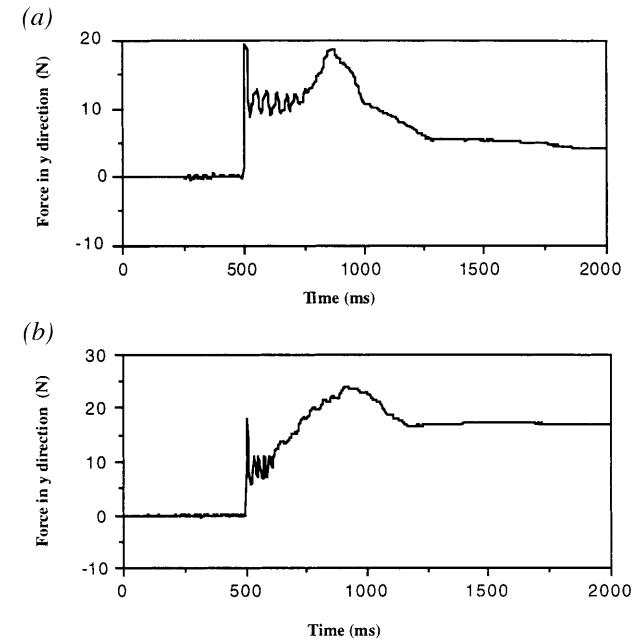

Fig. 16. Experimental comparison of contact force in the *y*-direction (*a*) using constant speed insertion motion; (*b*) using varying speed insertion motion.

resumed following the varying speed profile (i.e. that for case *a* in Fig. 12). The result (Fig. 14*b*) shows that the excessive contact force was significantly reduced. The cycle times were examined and compared. For the constant speed motion, the insertion speed was constrained to be the same as the insertion speed (5%) to avoid excessive contact force/moment. The corresponding cycle time is estimated to be about 1 s. For the varying-speed insertion, on the other hand, the highest possible speed (100%) was used for the approaching stage, while a varying speed was used for the chamfer-crossing stage. Therefore, the cycle time is reduced to about 0.5 s. Similar results were obtained for torques about the *z*-axis. A comparative experimental result for constant- and varying-speed insertion motion is shown in Fig. 15 and it can be seen that a 50% reduction in overshooting at the initial contact is achieved by using the varying-speed insertion motion. Improvement of contact force overshooting in the *x*- and *y*-directions is not as marked as in the *z*-direction (Fig. 16) because the insertion takes place in the *z*-direction and it has the most direct impact on the contact force.

5. Conclusions

If the intrinsic compliance of a robot is known to be adequate for a part mating application, other methods such as using additional compliance or active force sensing and control may not be necessary or may not be the most cost effective. Therefore, intrinsic compliance should always be explored first. The robot inertia affects its response to contact force/moment incurred during part mating. Such a response has been modelled to determine the insertion rate at which only contact force and moment free of overshooting will occur. The investigation led to the synthesis of a varying-speed insertion motion. It is shown through simulation and experiments that, with the varying-speed insertion motion, not only are contact force and moment limited and thus impact is improved, but also a shorter cycle time is achieved. In order to synthesise a varying-speed insertion motion reliably, knowledge about robot geometrical and dynamic parameters is necessary.

References

1. Y. L. Yao, “Transient lateral motion of robots in part mating, Robotic and Computer-Integrated Manufacturing”, 8(2), pp. 103–111, 1991.
2. M. C. Leu and Y. L. Jia, “Mating of rigid parts by a manipulator with its own compliance”, Transactions ASME, Journal of Engineering for Industry, 117(2), pp. 240–247, 1995.
3. H. A. ElMaraghy, W. H. ElMaraghy and L. Knoll, “Design specification of parts dimensional tolerance for robotic assembly”, Computers in Industry, 10, p. 47, 1988.
4. J. L. Nevins and D. E. Whitney, “Assembly Automation”, Automatica, Vol. 16, pp. 595–613, 1980.
5. H. Asada and Y. Kakumoto, “The dynamic RCC hand for high-speed assembly”, Proceedings IEEE International Conference on Robotics and Automation, PA, p. 120, 1988.
6. S. N. Gottschlich and A. C. Kak, “A dynamic approach to high-precision parts mating”, Proceedings IEEE International Conference on Robotics and Automation, PA, p. 1246, 1988.
7. Th. Meitinger and F. Pfeiffer, “Dynamic simulation of assembly processes”, Proceedings IEEE International Conference on Intelligent Robots and Systems, Part 2 (of 3), 5–9 August 1995, vol. 2, pp. 298–304, 1995.
8. T. Arai and H. Makino, “Analysis of part insertion with complicated shapes”, Annals CIRP, 38, p. 17, 1989.
9. M. E. Caine, T. Lozano-Perez and W. P. Seering, “Assembly strategies for chamferless parts”, Proceedings IEEE International Conference on Robotics and Automation, PA, p. 472, 1989.

10. D. R. Strip, "Insertion using geometric analysis and hybrid force-position control: Method and analysis", Proceedings IEEE International Conference on Robotics and Automation, PA, p. 1744, 1988.
11. D. R. Strip, "A passive mechanism for insertion of convex pegs", Proceedings IEEE International Conference on Robotics and Automation, PA, p. 242, 1989.
12. M. H. Wu and S. Hopkins, "Strategy for automatic assembly of spline peg hole based on stiffness hybrid control", 10th International Conference on Assembly Automation, PA, p. 95, 1989.
13. R. H. Sturges and S. Laowattana, "Passive assembly of non-axisymmetric rigid parts", Proceedings of the IEEE/RSJ/GI International Conference on Intelligent Robots and Systems, Part 2 (of 3) 12–16 September 1994, vol. 2, pp. 1218–1225, 1994.
14. R. H. Sturges and S. Laowattana, "Fine motion planning through constraint network analysis", Proceedings of the IEEE International Symposium on Assembly and Task Planning, 10–11 August 1995, pp. 160–170, 1995.
15. R. H. Sturges and S. Laowattana, "Design of an orthogonal compliance for polygonal peg insertion", Transactions ASME Journal of Mechanical Design, 118(1), pp. 106–114, 1996.
16. M. Leu, V. Dukovski and K. K. Wang, "Effect of mechanical compliance on deflection of robot manipulators", Annals CIRP, 36, pp. 305–309, 1987.

Appendix

A.1

In Eq. (5), $\mathbf{M}(\theta)$ is a 3×3 symmetric matrix

$$\mathbf{M}(\theta) = \begin{bmatrix} m_{11} & m_{12} & m_{13} \\ m_{21} & m_{22} & m_{23} \\ m_{31} & m_{32} & m_{33} \end{bmatrix}$$

where

$$\begin{aligned} m_{11} &= (m_1 a_1^{*2} + I_1) + (m_2 a_1^2 + m_2 a_2^{*2} + 2m_2 a_1 a_2^* c_2 + I_2) \\ &\quad + (m_3 a_1^2 + m_3 a_2^2 + 2m_3 a_1 a_2 c_2 + I_3) \\ m_{12} &= m_{21} = (m_2 a_2^{*2} + m_2 a_1 a_2^* c_2 + I_2) \\ &\quad + (m_3 a_2^2 + m_3 a_1 a_2 c_2 + I_3) \\ m_{13} &= m_{31} = -I_3, \quad m_{23} = m_{32} = -I_3 \\ m_{22} &= (m_2 a_2^{*2} + I_2) + (m_3 a_2^2 + I_3) \\ m_{13} &= +I_3 \end{aligned}$$

where m_i, a_i, a_i^* and I_i are the mass, length, location of the centre of gravity and moment of inertia of link i as shown in Fig. 5.

$\mathbf{V}$ is a 3×1 vector of centrifugal and Coriolis terms where

$$\begin{aligned} v_1 &= -\dot{\theta}_2^2(m_2 a_1 a_2^* s_2 + m_3 a_1 a_2 s_2) \\ &\quad -\dot{\theta}_1\dot{\theta}_2(2m_2 a_1 a_2^* s_2 + 2m_3 a_1 a_2 s_2) \\ v_2 &= \dot{\theta}_1^2(m_2 a_1 a_2^* s_2 + m_3 a_1 a_2 s_2), \quad v_3 = 0 \end{aligned}$$

A.2

The inertia and geometric parameters of the IBM 7545 robot:

$$\begin{aligned} &m_1 = 12.7 \text{ kg}, \quad m_2 = 4.35 \text{ kg}, \quad m_3 = 1.34 \text{ kg} \\ &I_1 = 0.454 \text{ kg } m^2, \quad I_2 = 0.0428 \text{ kg m}^2, \\ &\quad I_3 = 2.27 \times 10^{-4} \text{ kg m}^2 \\ &a_1 = 0.4 \text{ m}, \quad a_2 = 0.25 \text{ m}, \quad a_1^* = 0.153 \text{ m}, \\ &\quad a_2^* = 0.084 \text{ m} \\ &k_1 = 36\,722 \text{ N m rad}^{-1}, \; k_2 = 8878 \text{ N m rad}^{-1}, \\ &k_3 = 4500 \text{ N m rad}^{-1} \end{aligned}$$

A.3

In Eqs (8) to (10), $\mathbf{J}_H(t)$ is the Jacobian matrix expressed in the hand coordinate system $\{H\}$ and given by

$$\mathbf{J}_H(t) = \begin{bmatrix} j_{11} & j_{12} & 0 \\ j_{21} & j_{22} & 0 \\ -1 & -1 & -1 \end{bmatrix}$$

where

$$\begin{aligned} j_{11} &= a_1 s_{23} + a_2 s_3, \quad j_{12} = a_2 s_3, \\ j_{21} &= -a_1 c_{23} - a_2 c_3, \quad j_{22} = -a_2 c_3 \end{aligned}$$